

Demonstration of high-*Q* mid-infrared chalcogenide glass-on-silicon resonators

Hongtao Lin,¹ Lan Li,¹ Yi Zou,¹ Sylvain Danto,² J. David Musgraves,² Kathleen Richardson,² Stephen Kozacik,³ Maciej Murakowski,³ Dennis Prather,³ Pao T. Lin,⁴ Vivek Singh,⁴ Anu Agarwal,⁴ Lionel C. Kimerling,⁴ and Juejun Hu^{1,*}

¹Department of Materials Science and Engineering, University of Delaware, Newark, Delaware 19716, USA

²College of Optics & Photonics, Department of Materials Science and Engineering, University of Central Florida, Orlando, Florida 32816, USA

³Department of Electrical and Computer Engineering, University of Delaware, Newark, Delaware 19716, USA

⁴Department of Materials Science and Engineering, Massachusetts Institute of Technology, Cambridge, Massachusetts 02139, USA

*Corresponding author: hujuejun@udel.edu

Received February 20, 2013; revised March 18, 2013; accepted March 26, 2013;
posted March 27, 2013 (Doc. ID 185670); published April 26, 2013

We demonstrated high-index-contrast, waveguide-coupled As_2Se_3 chalcogenide glass resonators monolithically integrated on silicon fabricated using optical lithography and a lift-off process. The resonators exhibited a high intrinsic quality factor of 2×10^5 at $5.2 \mu\text{m}$ wavelength, which is among the highest values reported in on-chip mid-infrared (mid-IR) photonic devices. The resonator can serve as a key building block for mid-IR planar photonic circuits. © 2013 Optical Society of America

OCIS codes: (230.5750) Resonators; (130.3060) Infrared; (130.3120) Integrated optics devices.
<http://dx.doi.org/10.1364/OL.38.001470>

Owing to their strong optical confinement and long cavity photon lifetime, planar photonic resonators are recognized as key components for mid-infrared (mid-IR, 3–20 μm) applications, including spectroscopic sensing, free space communications, and thermal imaging [1]. Since silica becomes opaque at wavelengths longer than 3.5 μm , mid-IR integrated resonators demonstrated to date either involve special suspended designs [2–4] or new material platforms, such as silicon-on-sapphire [5,6]. Quality factors measured in these devices range from 3000 to 2.8×10^5 . However, bound by the onset of phonon absorption in crystalline silicon, the optical transparency window of these devices extends only up to 7 μm wavelength.

Alternatively, chalcogenide glasses (ChGs), namely the amorphous compounds containing S, Se, and/or Te, have been recognized as a material of choice for IR applications given their wide optical transparency window in the mid-IR [7]. Besides their excellent mid-IR transparency, ChGs possess low thermal conductivity ($<1 \text{ W/mK}$), large thermo-optic coefficients ($>10^{-4}/\text{K}$), and hence a photothermal figure-of-merit >300 times higher than silicon, making them ideal material candidates for on-chip photothermal detection down to single chemical molecule levels [8,9]. ChG mid-IR waveguides have been fabricated on silicon using photosensitive writing [10] and on exotic substrates, such as As_2S_3 glass [11], NaCl [12,13], and LiNbO_3 [14]. However, mid-IR ChG resonators have not yet been demonstrated.

In this Letter, we report for the first time ChG mid-IR resonators monolithically fabricated on a silicon platform by optical lithography. We chose As_2Se_3 over more commonly used sulfide ChGs given its high refractive index ($n \sim 2.66$ the mid-IR) [15] and reduced phonon energy, which gives rise to a long wavelength absorption onset up to 14 μm . The devices were tested by fiber end fire coupling using a quantum cascade laser (QCL) at 5.2 μm mid-IR wavelength.

Figure 1 schematically illustrates the fabrication process of the ChG mid-IR waveguide-coupled resonators, which was carried out at the Nanofabrication Facility at the University of Delaware. The devices were fabricated on 3" silicon wafers topped with 300 nm thermal oxide (from University Wafer) as the starting substrate. To prevent absorption of silica (extinction coefficient $k \sim 5.49 \times 10^{-3}$ at 5.2 μm [16]) and optical leakage into the silicon substrate, a 3 μm thick mid-IR transparent (up to 12 μm wavelength) and relatively low refractive index ($n \sim 2.1$) $\text{Ge}_{23}\text{Sb}_7\text{S}_{70}$ glass film [17] was first deposited as the bottom cladding. Details of the glass synthesis

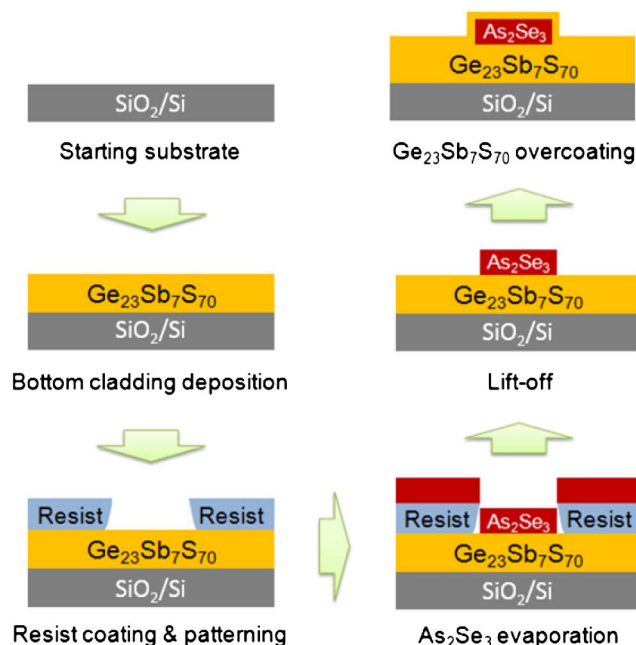


Fig. 1. Schematic fabrication process flow for the As_2Se_3 mid-IR waveguides (not drawn to scale).

and deposition processes can be found in [18,19]. Reversed patterns in a negative tone photoresist (NR9-1500PY, Futurrex Inc.) were defined using contact lithography on an ABM Mask Aligner, and a 1.1 μm thick As_2Se_3 film was subsequently deposited as the waveguide core layer. The entire structure was then sonicated in acetone to dissolve the resist layer beneath the undesired parts of the As_2Se_3 film, leaving an As_2Se_3 pattern reverse to that of the photoresist. As a final step, a 2 μm thick $\text{Ge}_{23}\text{Sb}_7\text{S}_{70}$ overcoating layer was deposited on top of the As_2Se_3 core to prevent surface oxidation and formation of large AsO_x crystallites [20]. To facilitate optical coupling into and out of the bus waveguides, the processed wafers were subsequently cleaved to form end facets.

Mid-IR transmission characteristics of the resonators were measured using a fiber end fire coupling method. Figure 2 illustrates a schematic diagram of the mid-IR measurement setup. In our measurements, a CaF_2 lens (NA ~ 0.25) was used to couple TE-polarized mid-IR light from a 5.2 μm external cavity tunable QCL (Daylight Solution, Inc.) into a customized InF_3 fiber (IRPhotonics Inc.). Since the optical fiber is multimode at the 5.2 μm wavelength (core/cladding diameters 40/150 μm), careful optimization of the laser-fiber alignment was performed to minimize excitation of high-order fiber modes. The mid-IR light was butt-coupled to the planar As_2Se_3 bus waveguides through the optical fiber [Fig. 3(a)], and optical output at the waveguide end facet was collected by another CaF_2 lens and imaged in the far field using a liquid nitrogen cooled InSb focal plane array (FPA). To minimize thermal radiation noise from the ambient background, a liquid nitrogen cooled bandpass filter centered at 5.2 μm wavelength was inserted in the optical path.

Subwavelength waveguide core dimensions (width 2.5 μm and height 1.1 μm) are necessary for single-mode operation and efficient coupling into the resonator given the high refractive index of As_2Se_3 . As is shown in Fig. 3(a), an adiabatic lateral taper section was inserted near the bus waveguide input facet to minimize coupling loss due to mode mismatch between the input fiber and the single-mode bus waveguide. A lateral offset of 5 mm between the input and output facets of the waveguides was added to prevent interference of the guided mode with stray free-space light directly from the laser. A far-field image of the guided mode from a 2.5 μm wide single-mode As_2Se_3 bus waveguide is shown in Fig. 3(b). The transmitted intensity was measured by integrating the number of counts on FPA pixels over the waveguide mode image, after subtraction of the thermal background contribution.

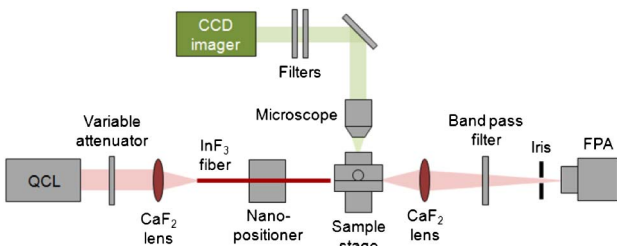


Fig. 2. Mid-IR fiber end fire waveguide measurement setup schematic.

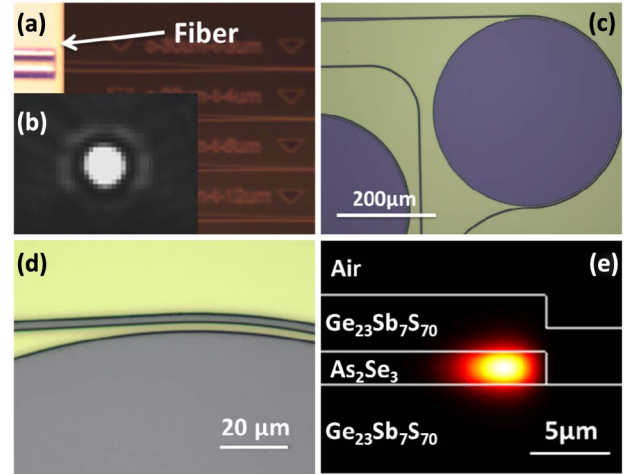


Fig. 3. (a) Top-view microscope image of a mid-IR InF_3 fiber end-coupled to an As_2Se_3 waveguide with a lateral taper to reduce the mode mismatch; (b) far-field image of the TE-guided mode from a single-mode As_2Se_3 bus waveguide; (c) optical microscope top-view image of a 200 μm radius mid-IR resonator; (d) microscope image showing the 2.75 μm wide coupling gap between the bus waveguide and the microdisk resonator; and (e) simulated field intensity profile of the fundamental whispering gallery mode of the ChG microdisk resonator.

Figure 3(c) shows the top view of a 200 μm radius pulley-coupled As_2Se_3 mid-IR microdisk resonator. The gap width between the disk and the single-mode bus waveguide is set to 2.75 μm to attain near-critical coupling operation [Fig. 3(d)]. Compared to the conventional coupler configuration, the pulley coupler design improves the fabrication tolerance by increasing the coupling strength [21,22]. Figure 4(a) shows the TE polarization transmission spectrum of the resonator. The group index calculated from the free spectral range (experimentally measured FSR ~ 8.16 nm) is 2.63, which is close to our finite difference simulation result (2.68) assuming a fundamental transverse whispering gallery mode order [Fig. 3(e)] of the disk resonator. Loaded Q factors, measured from 22 resonant peaks in three different samples, range from 6×10^4 to 10^5 . Figure 4(b) shows the spectrum measured from the highest Q device near its resonance peak at 5157.9 nm wavelength. A loaded Q factor of 10^5 was inferred from the spectrum, corresponding to an intrinsic Q factor of 2×10^5 and an equivalent waveguide propagation loss of 0.7 dB/cm. This Q factor is among the highest values reported in experimentally demonstrated mid-IR resonators.

We further performed full vectorial finite difference simulations [23] to quantify the optical loss mechanisms in the resonator. Figure 3(e) shows the calculated fundamental quasi-TE whispering gallery mode profile. The simulation indicates negligible optical loss (< 0.01 dB/cm) due to silica absorption, substrate leakage, and radiative bending loss. We consequently conclude that the loss must primarily result from either material absorption or sidewall roughness scattering. It is likely that excess surface roughness at the interface between the core and the top cladding layer accounts for the observed 0.7 dB/cm optical loss. Improvement of the resonator performance is thus expected through further processing optimization, or via adoption of

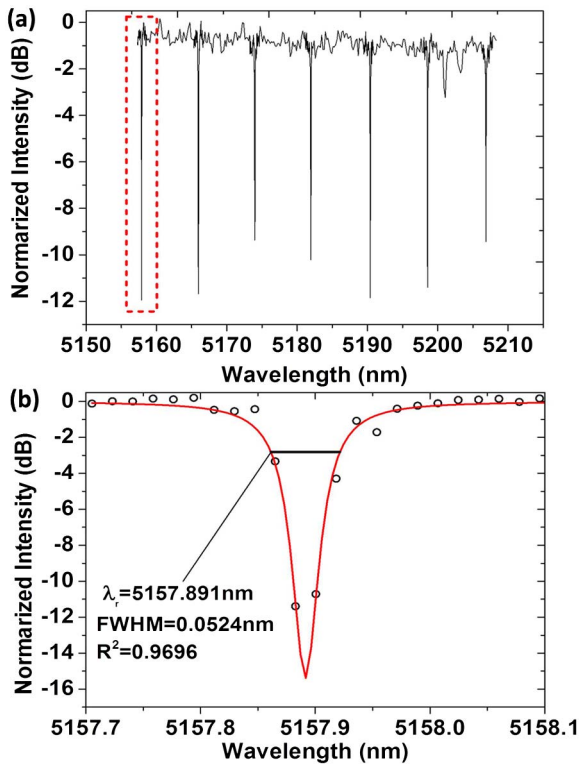


Fig. 4. (a) Mid-IR optical transmission spectrum of the As_2Se_3 microdisk resonator measured using a wavelength sweeping method and (b) spectrum near the optical resonance at 5157.89 nm wavelength (the red box in a). The dots are experimentally measured data and the line is the linear-scale Lorentzian fit, which indicates a loaded cavity quality factor of 10^5 .

fine-line patterning methods, such as electron beam lithography.

In conclusion, we have demonstrated for the first time ChG mid-IR microresonators monolithically integrated on silicon. We measured an intrinsic Q factor of 2×10^5 at 5.2 μm wavelength, which corresponds to a low propagation loss of 0.7 dB/cm. The high- Q ChG mid-IR resonator offers a promising device platform for mid-IR integrated photonics.

The authors gratefully acknowledge support from the National Science Foundation under award number 1200406 and EPSCoR grant EPS-0814251. Additional partial support has been provided by the U.S. Department of Energy [Contract No. DE-NA000421], NNSA/DNN R&D. This Letter has been prepared as an account of work partially supported by an agency of the United States Government. Neither the United States Government nor any agency thereof, nor any of their employees, makes any warranty, express or implied, or assumes any legal liability or responsibility for the accuracy, completeness or usefulness of any information, apparatus,

product or process disclosed, or represents that its use would not infringe privately owned rights. Reference herein to any specific commercial product, process, or service by trade name, trademark, manufacturer, or otherwise does not necessarily constitute or imply its endorsement, recommendation, or favoring by the United States Government or any agency thereof. The views and opinions of authors expressed herein do not necessarily state or reflect those of the United States Government or any agency thereof.

References

1. R. A. Soref, Proc. SPIE **6898**, 689809 (2008).
2. R. Shankar, R. Leijssen, I. Bulu, and M. Loncar, Opt. Express **19**, 5579 (2011).
3. R. Shankar, I. Bulu, R. Leijssen, and M. Loncar, Opt. Express **19**, 24828 (2011).
4. Z. Cheng, X. Chen, C. Y. Wong, K. Xu, and H. K. Tsang, IEEE Photonics J. **4**, 1510 (2012).
5. A. Spott, Y. Liu, T. Baehr-Jones, R. Ilic, and M. Hochberg, Appl. Phys. Lett. **97**, 213501 (2010).
6. R. Shankar, I. Bulu, and M. Loncar, Appl. Phys. Lett. **102**, 051108 (2013).
7. A. B. Seddon, J. Non-Cryst. Solids **184**, 44 (1995).
8. J. J. Hu, Opt. Express **18**, 22174 (2010).
9. H. T. Lin, Z. Yi, and J. J. Hu, Opt. Lett. **37**, 1304 (2012).
10. N. Ho, M. C. Phillips, H. Qiao, P. J. Allen, K. Krishnaswami, B. J. Riley, T. L. Myers, and N. C. Anheier, Opt. Lett. **31**, 1860 (2006).
11. C. Vigreux-Bercovici, E. Bonhomme, A. Pradel, J. E. Broquin, L. Labadie, and P. Kern, Appl. Phys. Lett. **90**, 011110 (2007).
12. C. Tsay, E. Mujagic, C. K. Madsen, C. F. Gmachl, and C. B. Arnold, Opt. Express **18**, 15523 (2010).
13. C. Tsay, Y. Zha, and C. B. Arnold, Opt. Express **18**, 26744 (2010).
14. X. Xia, Q. Chen, C. Tsay, C. B. Arnold, and C. K. Madsen, Opt. Lett. **35**, 3228 (2010).
15. N. Carlie, J. N. C. Anheier, H. A. Qiao, B. Bernacki, M. C. Phillips, L. Petit, J. D. Musgraves, and K. Richardson, Rev. Sci. Instrum. **82**, 053103 (2011).
16. E. D. Palik, *Handbook of Optical Constants of Solids* (Elsevier, 1997).
17. J. D. Musgraves, N. Carlie, J. Hu, L. Petit, A. Agarwal, L. C. Kimerling, and K. A. Richardson, Acta Mater. **59**, 5032 (2011).
18. L. Petit, N. Carlie, F. Adamietz, M. Couzi, V. Rodriguez, and K. C. Richardson, Mater. Chem. Phys. **97**, 64 (2006).
19. J. J. Hu, V. Tarasov, A. Agarwal, L. Kimerling, N. Carlie, L. Petit, and K. Richardson, Opt. Express **15**, 2307 (2007).
20. Y. Zou, H. Lin, O. Ogbuu, L. Li, S. Danto, S. Novak, J. Novak, J. D. Musgraves, K. Richardson, and J. Hu, Opt. Mater. Express **2**, 1723 (2012).
21. J. J. Hu, N. Carlie, N. N. Feng, L. Petit, A. Agarwal, K. Richardson, and L. Kimerling, Opt. Lett. **33**, 2500 (2008).
22. E. S. Hosseini, S. Yegnanarayanan, A. H. Atabaki, M. Soltani, and A. Adibi, Opt. Express **18**, 2127 (2010).
23. Photon Design Ltd., "<http://www.photond.com/products/fimmwave.htm>", retrieved.